AD-A097 997 NAVAL RESEARCH LAB WASHINGTON DC F/G 20/8
GENERATION AND IMPROVEMENT OF THE GYROTRON ELECTRON BEAM IN A B--ETC(U)
APR 81 C KYLER, K R CHU DE-AI01-80-ER-52065
UNCLASSIFIED NRL-MR-4401 NL

END
DATE FILMED
8-81
DTIC

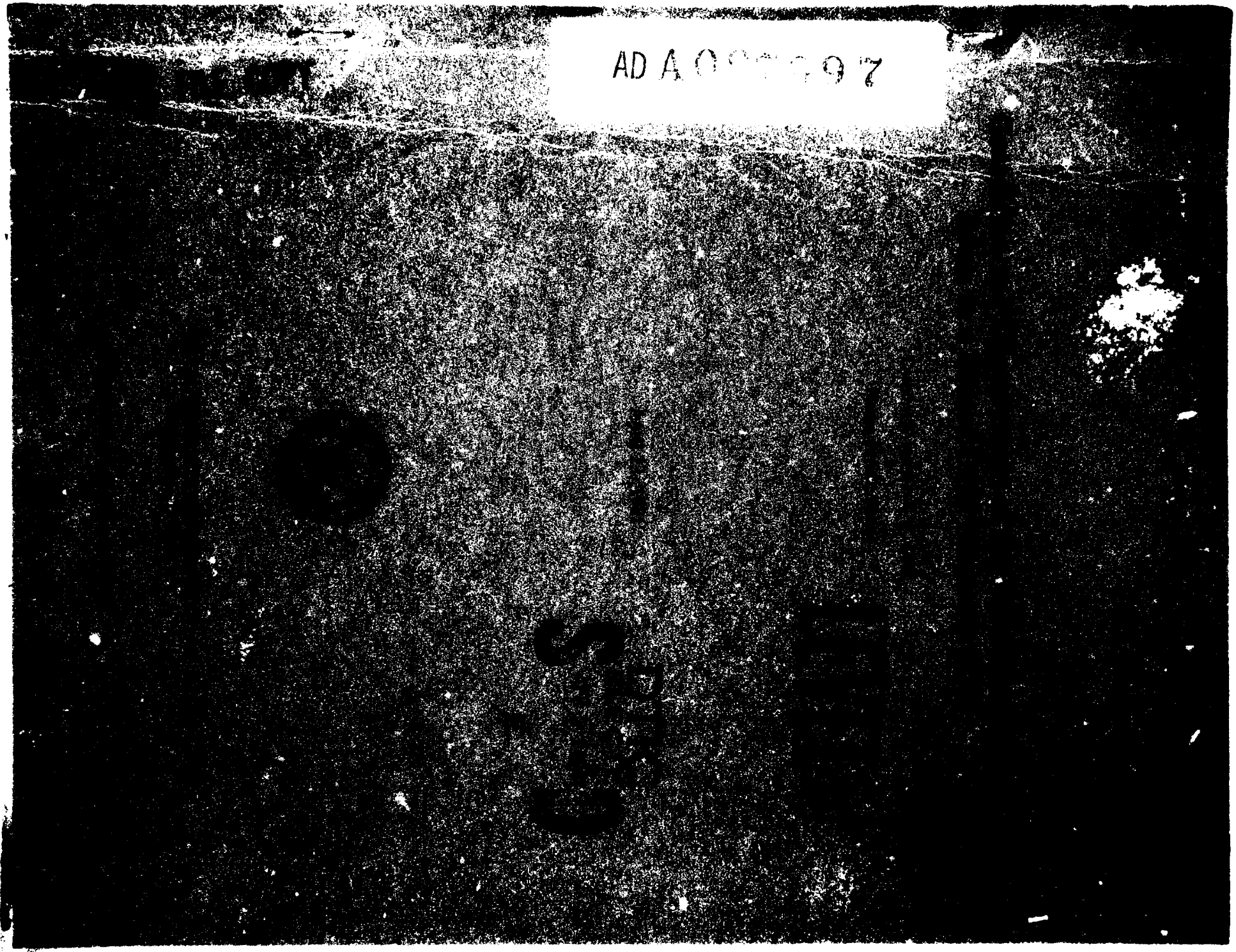
AD A0[illegible]97

SECURITY CLASSIFICATION OF THIS PAGE (When Data Entered)

(14) NRL-MR-4401

(9) REPORT DOCUMENTATION PAGE

READ INSTRUCTIONS BEFORE COMPLETING FORM

1. REPORT NUMBER
NRL Memorandum Report 4401

2. GOVT ACCESSION NO.
AD-A097997

3. RECIPIENT'S CATALOG NUMBER

4. TITLE (and Subtitle)
GENERATION AND IMPROVEMENT OF THE GYROTRON ELECTRON BEAM IN A BIASED CUSP MAGNETIC FIELD

5. TYPE OF REPORT & PERIOD COVERED
Interim report on a continuing NRL problem.

6. PERFORMING ORG. REPORT NUMBER

7. AUTHOR(s)
(10) Carolyn Kyler [redacted] K.R. Chu

8. CONTRACT OR GRANT NUMBER(s)
(15) DE-AI[illegible]-80-ER-[illegible]065

9. PERFORMING ORGANIZATION NAME AND ADDRESS
Naval Research Laboratory
Washington, D.C. 20375

10. PROGRAM ELEMENT, PROJECT, TASK AREA & WORK UNIT NUMBERS
DE-AI01-80ER52065
47-0865-0-1

11. CONTROLLING OFFICE NAME AND ADDRESS
Department of Energy*
Washington, D.C. 20545

(11) 22

12. REPORT DATE
Apr[redacted]81

13. NUMBER OF PAGES
22

14. MONITORING AGENCY NAME & ADDRESS(if different from Controlling Office)
(12) 23

15. SECURITY CLASS. (of this report)
UNCLASSIFIED

15a. DECLASSIFICATION/DOWNGRADING SCHEDULE

16. DISTRIBUTION STATEMENT (of this Report)
Approved for public release; distribution unlimited.

17. DISTRIBUTION STATEMENT (of the abstract entered in Block 20, if different from Report)

18. SUPPLEMENTARY NOTES
*Office of Naval Research, NRL Problem 47-0866-0-1,
Project No. RR0110941, Program Element No. 61153N.

19. KEY WORDS (Continue on reverse side if necessary and identify by block number)
Gyrotron electron beam
Biased cusp magnetic field

20. ABSTRACT (Continue on reverse side if necessary and identify by block number)
Transition of an electron beam through a biased magnetic cusp field can result in higher perpendicular-to-parallel velocity ratio or lower momentum spread. Analytical relations for the transformation of velocity ratio and momentum spread across the magnetic cusp are derived on the assumption of adiabatic electron motion. A single particle trajectory code is developed to investigate the nonadiabatic electron behavior in two models of a biased cusp magnetic field. After intensive data analysis, some general conclusions are presented on the prospects of generation and improvement of the gyrotron electron beam in a biased cusp magnetic field.

DD FORM 1 JAN 73 1473 EDITION OF 1 NOV 65 IS OBSOLETE
S/N 0102-014-6601

SECURITY CLASSIFICATION OF THIS PAGE (When Data Entered)

251 950

CONTENTS

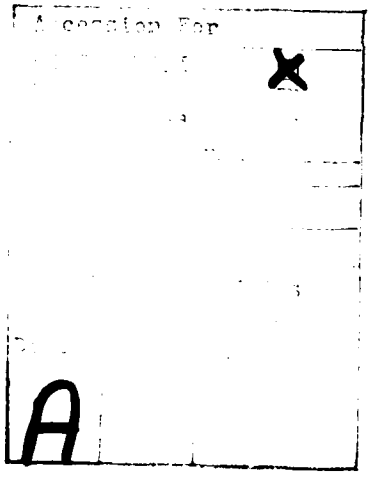

GENERATION AND IMPROVEMENT OF THE GYROTRON ELECTRON BEAM IN A BIASED CUSP MAGNETIC FIELD

I. INTRODUCTION

The present work is motivated by some recent interest in and proposed schemes for improving the qualities of the electron beam used in gyrotron devices. Ideally, a gyrotron electron beam should have the following properties:

(i) It is monoenergetic.

(ii) It is cold, that is, all the electrons have the same perpendicular velocity ($v_\perp$) and streaming velocity (v_z), where $v_\perp$ and v_z refer to velocities perpendicular and parallel to the applied magnetic field, respectively.

(iii) Most of the electron kinetic energy is in the form of transverse gyrational motion (i.e., $v_\perp >> v_z$). This is so because, in contrast to a TWT or klystron, the free energy in the gyrotrons resides in the electron gyrational motion rather than the streaming motion. A typical desirable case is $v_\perp \approx 2v_z$.

(iv) All the electrons have the same guiding center radius. Hence they experience the same wave field, and optimization could be accomplished for all of them.

Because of these requirements, electron guns developed for conventional microwave devices are generally unsuitable for use in gyrotrons. At present, the magnetron injection gun generates the best quality electron beam[1] and is commonly employed in gyrotrons.

Manuscript submitted on February 23, 1981.

Of the four requirements stated above, (i) is fairly easy to meet, but the remaining ones, added together, present considerable difficulties in the design of an electron gun. In particular, as will be shown in Sec. III, there is a trade-off between (ii) and (iii). For example, one could increase the velocity ratio $\alpha (\equiv v_\perp / v_z)$, at the cost of increased velocity spread, through adiabatic compression of the electron beam in a slowly rising magnetic field. This method has been suggested by Hirshfield[2] for enhancing the efficiency of gyromonotrons, which can tolerate relatively large velocity spread. An experimental test of this method is planned at Yale University. Conversely, for devices more sensitive to velocity spread, one could decompress the electron beam to reduce its velocity spread at the cost of reduced α. The magnetic decompression method has been suggested by Keren[3] for improving the gain and bandwidth of the slow wave cyclotron amplifier.

Recently, many researchers[4] have been looking into the possibility of converting a substantial part of the energy of a purely streaming beam (easily available from, for example, a Pierce electron gun) into a gyrational beam by passing it through a rapidly rising magnetic field gap. Preliminary experimental tests of this scheme are being carried out by Smith (Naval Research Laboratory),[5] Wachtel (Hebrew University),[5] and Hirshfield (Yale University).[5]

All the schemes described above employ a biased cusp magnetic field as profiled in Fig. 1. Electron motion is adiabatic or nonadiabatic in the transition region (of length L) depending on the number of gyrations the electron makes during the transition. The purpose of the present work is twofold. First, we derive some analytical formulae to examine the adiabatic compression and decompression of a gyrotron beam. It is shown that adiabatic compression of the beam is indeed a viable method for improving the efficiency of the gyromonotron. Second, we develop a single particle trajectory code to examine the nonadiabatic conversion of a streaming beam into a gyrating beam. We find that the generation of a good quality gyrotron beam requires a very thin streaming beam and a large magnetic field compression ratio. This conclusion is supported by extensive data taken with the simple trajectory code. However, a detailed assessment of the feasibility of such a scheme should be carried out with a full scale simulation code.[6]

II. MODEL

The motion of an electron in a static magnetic field **B** is governed by the equation

$$\frac{d}{dt}\,\mathbf{p} = -\frac{e}{\gamma mc}\,\mathbf{p}\times\mathbf{B}, \tag{1}$$

where $\gamma = (1 - v^2/c^2)^{-1/2}$, $\mathbf{p} = \gamma m\mathbf{v}$, and $\mathbf{v}$ is the velocity.

The magnetic field of interest is axisymmetric and has no azimuthal component, i.e.,

$$\mathbf{B}(r,z) = B_r(r,z)\mathbf{e}_r + B_z(r,z)\mathbf{e}_z,$$

where $B_r(r,z)$ and $B_z(r,z)$ can be expressed in terms of $B_z(0,z)$, the z-component of the magnetic field on the axis,[7]

$$B_r(r,z) = \sum_{n=1}^{\infty} \frac{(-1)^n}{n!(n-1)!}\left(\frac{r}{2}\right)^{2n-1} \frac{d^{2n-1}}{dz^{2n-1}}\,B_z(0,z), \tag{2}$$

$$B_z(r,z) = \sum_{n=0}^{\infty} \frac{(-1)^n}{(n!)^2}\left(\frac{r}{2}\right)^{2n} \frac{d^{2n}}{dz^{2n}}\,B_z(0,z), \tag{3}$$

The corresponding vector potential is

$$\mathbf{A}(r,z) = A_\theta(r,z)\,\mathbf{e}_\theta,$$

where

$$A_\theta(r,z) = \sum_{n=1}^{\infty} \frac{(-1)^{n-1}}{n!(n-1)!}\left(\frac{r}{2}\right)^{2n-1} \frac{d^{2n-2}}{dz^{2n-2}}\,B_z(0,z). \tag{4}$$

Thus **B** is uniquely specified by $B_z(0,z)$. In our numerical evaluation of the electron trajectory, two models of $B_z(0,z)$ are used: the hyperbolic tangent model and the Moster-Molnar model (Fig. 1), as described below:

(A) The hyperbolic tangent model is given by:

$$B_z(0,z) = \frac{1}{2}(B_1 + B_2) + \frac{1}{2}(B_2 - B_1)\tanh(z/L). \tag{5}$$

Substituting Eq. (5) into Eqs. (2)-(4) and retaining terms up to sixth order in r/L, we obtain

$$B_r(r,z) = (B_2 - B_1)\left[-\frac{1}{4}\left(\frac{r}{L}\right)\operatorname{sech}^2\frac{z}{L} + \frac{1}{16}\left(\frac{r}{L}\right)^3\left[2\tanh^2\frac{z}{L}\operatorname{sech}^2\frac{z}{L} - \operatorname{sech}^4\frac{z}{L}\right]\right.$$
$$\left. - \frac{1}{96}\left(\frac{r}{L}\right)^5\left[2\operatorname{sech}^6\frac{z}{L} - 11\operatorname{sech}^4\frac{z}{L}\tanh^2\frac{z}{L} + 2\tanh^4\frac{z}{L}\operatorname{sech}^2\frac{z}{L}\right]\right], \tag{6}$$

$$B_z(r,z) = \frac{1}{2}(B_1 + B_2) + (B_2 - B_1)\left[\frac{1}{2}\tanh\frac{z}{L} + \frac{1}{4}\left(\frac{r}{L}\right)^2 \operatorname{sech}^2\frac{z}{L}\tanh^2\frac{z}{L}\right.$$
$$+ \frac{1}{16}\left(\frac{r}{L}\right)^4\left[2\operatorname{sech}^4\frac{z}{L}\tanh\frac{z}{L} - \tanh^3\frac{z}{L}\operatorname{sech}^2\frac{z}{L}\right]$$
$$\left. + \frac{1}{288}\left(\frac{r}{L}\right)^6\left[17\operatorname{sech}^6\frac{z}{L}\tanh\frac{z}{L} + 26\operatorname{sech}^4\frac{z}{L}\tanh^3\frac{z}{L} - 2\operatorname{sech}^2\frac{z}{L}\tanh^5\frac{z}{L}\right]\right], \tag{7}$$

$$A_\theta(r,z) = \frac{r}{4}(B_1 + B_2) + (B_2 - B_1)\left[\frac{r}{4}\tanh\frac{z}{L}\right.$$
$$\left. + \frac{r}{16}\left(\frac{r}{L}\right)^2\operatorname{sech}^2\frac{z}{L}\tanh\frac{z}{L} + \frac{r}{96}\left(\frac{r}{L}\right)^4\cdot\left[2\operatorname{sech}^4\frac{z}{L}\tanh\frac{z}{L} - \tanh^3\frac{z}{L}\operatorname{sech}^2\frac{z}{L}\right]\right]. \tag{8}$$

(B) The Moster-Molnar model

The Moster-Molnar field is produced by two semi-infinite solenoids separated by a thin iron pole piece. The on-axis B_z field is given by

$$B_z(0,z) = (B_1 - B_2)\,F(z) + B_2, \tag{9}$$

where

$$F(z) = \begin{cases} \frac{1}{\pi}\left\{\tan^{-1}\left(\frac{L}{z}\right) - \frac{z}{L}\left[1 + \left(\frac{z}{L}\right)^2\right]^{-1}\right\}, & z \geqslant 0 \\ 1 - \frac{1}{\pi}\left\{\tan^{-1}\left(\frac{-L}{z}\right) + \frac{z}{L}\left[1 + \left(\frac{z}{L}\right)^2\right]^{-1}\right\}, & z < 0 \end{cases}$$

Substitution of Eq. (9) into Eqs. (2)-(4) gives

$$B_r(r,z) = \frac{1}{\pi}(B_1 - B_2)\left\{\frac{r}{L}\left[1 + \left(\frac{z}{L}\right)^2\right]^{-2} + \frac{1}{2}\left(\frac{r}{L}\right)^3\left[1 - 5\left(\frac{z}{L}\right)^2\right]\left[1 + \left(\frac{z}{L}\right)^2\right]^{-4}\right.$$
$$\left. + \frac{1}{8}\left(\frac{r}{L}\right)^5\left[3 - 42\left(\frac{z}{L}\right)^2 + 35\left(\frac{z}{L}\right)^4\right]\left[1 + \left(\frac{z}{L}\right)^2\right]^{-6}\right\}, \tag{10}$$

$$B_z(r,z) = (B_1 - B_2)\,F(z) + B_2$$
$$+ \frac{1}{\pi}(B_1 - B_2)\left(\frac{z}{L}\right)\left\{-2\left(\frac{r}{L}\right)^2\left[1 + \left(\frac{z}{L}\right)^2\right]^{-3} + \frac{3}{5}\left(\frac{r}{L}\right)^4\left[-3 + 5\left(\frac{z}{L}\right)^2\right]\left[1 + \left(\frac{z}{L}\right)^2\right]^{-5}\right.$$
$$\left. - \frac{5}{6}\left(\frac{r}{L}\right)^6\left[3 - 14\left(\frac{z}{L}\right)^2 + 7\left(\frac{z}{L}\right)^4\right]\left[+\left(\frac{z}{L}\right)^2\right]^{-7}\right\}, \tag{11}$$

$$A_\theta(r,z) = \frac{r}{2}\left[(B_1 - B_2)\,F(z) + B_2\right] + \frac{1}{\pi}(B_1 - B_2)\left(\frac{z}{L}\right)$$
$$\cdot\left\{-\frac{1}{2}\left(\frac{r}{L}\right)^3\left[1 + \left(\frac{z}{L}\right)^2\right]^{-3} + \frac{1}{8}\left(\frac{r}{L}\right)^5\left[-3 + 5\left(\frac{z}{L}\right)^2\right]\left[1 + \left(\frac{z}{L}\right)^2\right]^{-5}\right\}. \tag{12}$$

Figure 1 shows the hyperbolic tangent field [Eq. (5)] and the Moster-Molnar field [Eq. (9)] for the same values of B_1 and B_2. As can be seen, the two field profiles are similar, each approaching a constant value as $|z| \to \infty$. The two alternative fields allow one to check the sensitivity of results to profile changes.

In the two models, B_1 and B_2 are arbitrary constants. For the special case $B_1 = -B_2$, they reduce to the regular cusp magnetic field.[8]

Because of axisymmetry, the canonical angular momentum P_θ is conserved, where

$$P_\theta = \gamma m r v_\theta - erA_\theta/c.$$

Any inaccuracy due to either numerical errors or the truncation of the infinite sums in Eqs. (2)-(4) will result in the nonconservation of P_θ. Hence the degree of conservation of P_θ has been monitored to insure the accuracy of our calculations.

III. ADIABATIC COMPRESSION AND DECOMPRESSION OF THE ELECTRON BEAM

In Fig. 1, we assume that a monoenergetic electron beam propagates from left to right and restrict our consideration to the following two cases: (i) $B_2 > B_1 > 0$ (compression), and (ii) $B_1 > B_2 > 0$ (decompression). We also assume that the magnetic field observed by the electrons varies slowly (a small fractional change in one gyro-period) so that the electron magnetic momentum is conserved, i.e.,

$$p_{\perp 1}^2/B_1 = p_{\perp 2}^2/B_2, \tag{13}$$

where subscripts "1" and "2" refer to regions far to the left and the right of the transition region, respectively. Conservation of total kinetic momentum in a static magnetic field requires that

$$p_{\perp 1}^2 + p_{z1}^2 = p_{\perp 2}^2 + p_{z2}^2 \tag{14}$$

Combining Eqs. (13) and (14), we obtain

$$\begin{aligned} p_{z2}^2 &= p_{\perp 1}^2 + p_{z1}^2 - p_{\perp 1}^2 B_2/B_1, \\ &= p_{z1}^2 \, [1 + \alpha_1^2(1 - f)], \end{aligned} \tag{15}$$

where $\alpha = p_\perp/p_z$ and $f = B_2/B_1$. From Eqs. (13) and (15), we obtain

$$\alpha_2 = \alpha_1 f^{1/2} \, [1 + \alpha_1^2(1 - f)]^{-1/2}. \tag{16}$$

and

$$f = \frac{1+\alpha_1^2}{1+\alpha_2^2}\left(\frac{\alpha_2}{\alpha_1}\right)^2. \tag{17}$$

Eqs. (15)-(17) give

$$\begin{aligned} p_{z2} &= p_{z1}\,[1+\alpha_1^2\,(1-f)]^{1/2} \\ &= p_{z1}[(1+\alpha_1^2)/(1+\alpha_2^2)]^{1/2}. \end{aligned} \tag{18}$$

To relate the momentum spread in region 2 to that in region 1, we let $\Delta p_\perp$ and Δp_z be, respectively, the perpendicular and parallel momentum spreads of the electron beam and assume $\Delta p_\perp << p_\perp$, $\Delta p_z << \Delta p_z$. The monoenergetic assumption,

$$p_\perp^2 + p_z^2 = \text{constant} \tag{19}$$

then gives

$$\Delta p_z = \alpha\ \Delta p_\perp. \tag{20}$$

Using Eqs. (19), (20) and the first equality of Eq. (15), we obtain

$$\begin{aligned} p_{z2}\,\Delta\,p_{z2} &= f\,p_{\perp 1}\,\Delta p_{\perp 1} \\ &= f\,p_{\perp 1}\,\Delta p_{z1}/\alpha. \end{aligned} \tag{21}$$

Combining the second equality of Eq. (15) with Eqs. (16) and (21) gives

$$\frac{\Delta p_{z2}}{p_{z2}} = \left(\frac{\alpha_2}{\alpha_1}\right)^2 \frac{\Delta p_{z1}}{p_{z1}}. \tag{22}$$

Eliminating p_{z2} and p_{z1} in Eq. (22) with the aid of Eq. (18), we obtain

$$\Delta p_{z2} = \left(\frac{1+\alpha_1^2}{1+\alpha_2^2}\right)^{1/2} \frac{\alpha_2^2}{\alpha_1^2}\,\Delta p_{z1}. \tag{23}$$

Eqs. (22) and (23) show how the relative parallel momentum spread ($\Delta p_z/p_z$) and absolute parallel momentum spread (Δp_z) change as one varies the velocity ratio α through adiabatic compression. Since γ is the same for all the electrons, the parallel velocity spread varies in the same manner. In general, the higher the velocity ratio of the electron beam is, the higher its velocity spread will be. The parallel velocity (or momentum) spread is physically a more meaningful quantity than the perpendicular velocity spread because it causes individual electrons to see different Doppler shifted wave frequencies and consequently smears the wave-electron resonance.

From the definition of α, we can express the spread in α in terms of the spread in momentum as follows:

$$\frac{\Delta\alpha}{\alpha} = \left(1 + \frac{1}{\alpha^2}\right) \frac{\Delta p_z}{p_z}. \tag{24}$$

Finally, we note from Eq. (15) that the condition for electron reflection ($p_{z2} = 0$) is

$$f \geq 1 + 1/\alpha_1^2 \tag{25}$$

As an example, we apply the results of this section to a monoenergetic (70 *keV*) electron beam with $\alpha = 2$ and $\Delta p_z/p_z = 5\%$.[9] Theory[10] predicts that the maximum gyromonotron efficiency obtainable with this electron beam is ~67%. However if the beam is adiabatically compressed to $\alpha = 2.5$ before entering the interaction region, a maximum efficiency of ~78% is predicted. In the following, we examine the feasibility and requirements of such a scheme. Substituting $\alpha_2 = 2.5$ and $\alpha_1 = 2$ into Eq. (22), we find that the momentum spread after compression increases to 7.8%, still a negligibly low value for gyromonotrons. From Eq. (17), we obtain $f = 1.078$, i.e., it takes a 7.8% magnetic field increase to raise α from 2 to 2.5. It should be noted that in the interaction region (i.e., the cavity) there will be an additional magnetic field increase of ~8% for the purpose of efficiency optimization.[10] Thus, the electron beam will experience a total magnetic field increase of ~16%. The question then arises whether some of the beam electrons will be reflected. Substituting $\alpha = 2$ and $\Delta p_z/p_z = 5\%$ into Eq. (24), we obtain $\Delta\alpha = 0.125$. Thus, we can crudely estimate that α of the uncompressed electrons ranges from 1.875 to 2.125. It is the upper value we need to examine to determine whether there will be reflections. Substituting this value for α_1 into Eq. (25), we find that it requires a 22% magnetic field increase for the electrons with the highest α to be reflected, representing a safety margin of 6% provided a negligible portion of electrons lies beyond the assumed α range.

IV. NONADIABATIC CONVERSION OF ELECTRON PARALLEL ENERGY INTO PERPENDICULAR ENERGY

In this section, we examine the trajectory characteristics of a single electron in traversing a biased cusp magnetic field. The Moster-Molnar field given by Eqs. (10) and (10) will be used to model the

field (Fig. 1). We assume the electron energy to be 70 keV, a voltage representative of those commonly used in high power gyrotrons. Initially, the electron is at the far left of the cusp (Fig. 1) propagating axially toward the right at a distance of r_i from the axis. With B_1, B_2, L and r_i specified, Eq. (1) is then numerically integrated from $z/L << 0$ to $z/L >> 0$. A deferred limit integrating subroutine[11] is used which employs Richardson extrapolation to achieve higher order accuracy and has built-in error control. In all the calculations, P_θ is conserved to better than 10^{-4}, indicating good numerical accuracy.

The main quantity of interest is the electron velocity ratio α $(=v_\perp/v_z)$ after passing through the cusp. Figure 2 shows plots of α versus the initial electron radial position r_i for various values of B_1 and B_2. Note that r_i, B_1 and B_2 are all normalized to the transition distance L. Some general characteristics are summarized below.

(i) α is very sensitive to r_i. Hence an electron beam of zero momentum spread but finite cross section would end up with a momentum spread (Δp_z) at the right hand side of the cusp. As will be seen, this is a major limitation for the generation of a good quality gyrotron electron beam.

(ii) Low values of B_1 combined with high values of B_2 generally produce higher values of α (Fig. 2a-c). However, if the average magnetic field in the cusp region is so high that the electron makes more than one gyration, α starts to decrease (Fig. 2d-f).

(iii) If $B_1 < 0$, the electron encircles the axis after reaching the right hand ride of the cusp. Similarly, it touches the axis if $B_1 = 0$ and stays on one side of the axis if $B_1 > 0$. The case $B_1 \approx 0$ apparently will lead to a concentration of charge near the axis. Space charge effects have been demonstrated to be important in such a case.[12]

(iv) The Moster-Molnar field was used in obtaining Fig. 2. To examine the sensitivity of these results to profile variation, we have replaced the Moster-Molnar profile with the hyperbolic tangent profile, keeping everything else equal. It is found that α is generally lower, by as much as 30%, in the smoother hyperbolic tangent profile.

Turning now to the prospect of generating a good quality gyrotron beam by the use of the biased cusp magnetic field, we first consider a specific example — the data on Fig. 2d marked by $B_2L = 12\ kG \cdot \text{cm}$. We choose the point at $r_i/L = 0.35$ for which $\alpha = 0.1$. The slope of the curve near $r_i/L = 0.35$ gives the following relation:

$$\Delta\alpha/\alpha \simeq 3.3\ \Delta r/L, \tag{26}$$

where Δr is the thickness of the annular beam before entering the cusp (Fig. 3). Substituting $\alpha = 0.1$ and Eq. (26) into Eq. (24), we obtain the parallel momentum spread as a function of Δr,

$$\Delta p_z/p_z \simeq 3.27 \times 10^{-2}\ \Delta r/L. \tag{27}$$

For the gyrotrons, an α value of 2 is acceptable. Thus we need to raise the α value from 0.1 to 2 by adiabatically compressing the beam. Substituting $\alpha_1 = 0.1$ and $\alpha_2 = 2$ into Eq. (17), we find that the required magnetic field compression ratio is $f \simeq 80$. Hence the final magnetic field B_f is given by

$$B_fL = 960\ KG \cdot \text{cm} \tag{28}$$

and from Eq. (22) and (27), the final momentum spread is

$$\Delta p_z/p_z \simeq 13.1\ \Delta r/L \tag{29}$$

In the abcve example, all quantities are normalized to L. Thus, we have the flexibility of choosing a specific value of B_f. Letting $B_f = 50$ kG, we obtain $L = 19.2$ cm, $B_1 = 0.104$ kG, $B_2 = 0.625$ kG, and $r_i = 6.72$ cm. Finally, if the allowable momentum spread ($\Delta p_z/p_z$) is 7.5%, Δr as obtained from Eq. (29) is 0.1 cm. Hence the total cross section of the beam is

$$A = 2\pi r_i\ \Delta r \simeq 4.6\ \text{cm}^2.$$

Assuming a current density of $5A/\text{cm}^2$, a total beam current of 23 A could be achieved.

Beams generated from thermonic cathode are usually limited in current density. The operation of a gyrotron, however, often requires a high current electron beam. Thus, the cross-sectional area (A) of the initial beam is a good measure of the merit of the beam generation scheme discussed above. Since $A = 2\pi r_i\ \Delta r$, A could be enlarged by increasing either the beam thickness Δr or the beam radius r_i. As Fig. 2 indicates, increasing Δr would lead to an increase in momentum spread. On the other hand, increasing r_i would require a large magnetic field compression ratio (following the cusp) to bring the

radius down. It is seen from Eq. (22) that large magnetic compression ratio also tends to amplify whatever momentum spread the beam has acquired in the cusp. Thus, either method for enlarging the beam cross-sectional area degrades the quality of the beam. The issue is then which method produces less spoiling effect. This is best resolved with a broad survey of the data shown in Fig. 2. Table I lists many more examples obtained in the same manner and subject to the same requirements as in the above example (i.e, $\alpha = 2$, $\Delta p_z/p_z = 7.5\%$, and $B_f = 50$ kG). The entries are listed in descending order of the initial cross sectional area A. As mentioned earlier, B_f in Table I was arbitrarily chosen to be 50 kG. The same beam parameters ($\alpha = 2$, $\Delta p_z/p_z = 7.5\%$) could be achieved in a smaller (or larger) magnetic field provided B_1 and B_2 are smaller (or larger) and r_i, Δr, L, and r_f are larger (or smaller) by the same factor.

As we observe from Table I, although there are slight deviations from case to case, the general trends are that (i) to obtain a good quality beam, one always has to start with a thin beam (i.e., $\Delta r << r_i$) independent of the cross-sectional area needed, and (ii) to obtain a high current beam with the same quality, a large magnetic field compression is necessary (i.e., small B_1 and B_2, recalling $B_f = 50$ kG for all data).

Using an idealized, infinitely sharp cusp, Baird and Attard[13] have derived a useful generic relation,

$$\frac{\Delta p_z}{p_z} = \alpha^2 \frac{\Delta r}{r_i} \tag{30}$$

which predicts the minimum achievable momentum spread as a function of α, Δr, and r_i. The results presented in Table I indicate a momentum spread approximately 1.1 to 1.7 times larger than what Eq. (30) predicts due to the finite width of the cusp.

V. SUMMARY AND DISCUSSION

We have shown in Sec. III that a typical gyrotron beam available today ($\alpha \leq \Delta p_z/p_z \leq 10\%$) could be improved by the method of adiabatic magnetic compression for high efficiency operation of gyromonotrons. The idea is to trade the momentum spread, which at 10% represents a high safety

margin for gyromonotrons, for higher velocity ratio (α) and consequently higher efficiency. In Sec. IV, we have drawn some general conclusions on the generation of gyrotron beams through biased cusp magnetic field. These conclusions are based on a simplified model in which the space charge effect is neglected, and, further, the initial electron beam is assumed to be cold ($\Delta p_z = 0$). In most cases of interest to microwave devices, the beam space charge effect is of higher order. It is also well known that electron beams generated from a Pierce electron gun can indeed have very small momentum spread. Although these facts lend some credibility to our general conclusions, we emphasize that our quantitive results are not suitable for use as design parameters. Rather, they serve as a useful guide for full scale simulations in which the beam space charge effect as well as the initial momentum spread could be accounted for. A final design of the gyrotron electron gun awaits the results of such full scale simulations.

The authors would like to acknowledge many helpful discussions with Drs. J. M. Baird, D. Dialetis, A. T. Drobot, Y. Y. Lau, M. E. Read, and S. Smith. C. Kyler would also like to thank Drs. J. Brown, R. Parker, and B. Lotze for arranging a summer research position at NRL. This work was supported by Dept. of Energy (Contract DE-AI01-80ER52065) and Office of Naval Research (Contract N00014-80-C-0075).

REFERENCES

1. The magnetron injection gun was first used in gyrotrons by researchers in the Soviet Union. A numerical simulation of the magnetron injection gun can be found in J.L. Seftor, A.T. Drobot, and K.R. Chu, "An Investigation of a Magnetron Injection Gun Suitable for Use in Cyclotron Resonance Masers," IEEE Trans. ED-26, 1609-1616 (1979).

2. J.L. Hirshfield, private communication.

3. H. Keren, private communication.

4. O. Dohler and S. Smith (private communication), J.L. Hirshfield and J.M. Wachtel (private communication), S. Ahn (to be published), J.M. Baird and A.E. Attard ("Interim Report on the Electron Gun Study Program," July, 1980), A.T. Drobot (to be published), and N.R. Vanderplaats (to be published).

5. Private communications.

6. See, for example, W.B. Herrmannsfeldt "Electron Trajectory Program " SLAC Rep. 166, Standford Linear Accelerator Center, 1973.

7. See, for example, V.K. Zworykin, G.A. Morton, E.G. Ramberg, J. Hillier, and A.W. Vance, "Electron Optics and the Electron Microscope," John Wiley and Sons, Inc. (New York, 1945), pp. 474-475.

8. A brief literature review on regular cusp magnetic field can be found in M.J. Rhee and W.W. Destler "Relativistic Electron Dynamics in a Cusped Magnetic Field," Phys. of Fluids *17*, 1574-1581 (1974).

9. These parameters are similar to those of the C-band electron gun designed and manufactured by Varian Associates.

10. K.R. Chu, M.E. Read, and A.K. Ganguly, "Methods of Efficiency Enhancement and Scaling for the Gyrotron Oscillator," IEEE Trans. MTT-28, 318-325 (1980).

11. J. Boris and N. Winsor, "Extrapolated Numerical Integration in Theory and Practice," Princeton Plasma Physics Laboratory, MATT-652 (Nov. 1970).

12. N.R. Vanderplaats, private communication.

13. J.M. Baird and A.E. Attard (see Ref. 4).

Table I. Various sets of parameters for achieving a 70 keV electron beam with $\alpha = 2$ and $\Delta p_z/p_z = 7.5\%$ in a magnetic field of 50 kG. Initially, the beam has no perpendicular momentum or momentum spread. After gaining a small $p_\perp$ (or α) in the biased cusp magnetic field, the beam is adiabatically compressed to reach the final α value (cf. Fig. 3).

A (cm^2)	r_i (cm)	Δr (cm)	B_i (kG)	B_2 (kG)	L (cm)	r_f (cm)
34.0	17.6	0.307	0.040	0.397	50.0	0.498
13.6	11.2	0.194	0.063	0.502	31.7	0.396
6.38	7.5	0.135	0.093	0.559	21.5	0.326
3.72	6.8	0.088	0.192	1.92	10.4	0.040
1.63	4.03	0.065	0.174	0.694	11.5	0.238
1.33	4.16	0.051	0.313	2.50	6.4	0.052
1.16	3.43	0.054	0.204	0.408	9.8	0.220
0.421	2.41	0.028	0.541	3.24	3.7	0.068
0.125	1.34	0.015	0.971	3.88	2.1	0.091
0.112	0.99	0.018	0.354	3.89	2.8	0.085
0.100	1.17	0.014	1.110	2.22	1.8	0.097
0.090	1.06	0.014	0.329	2.64	3.0	0.090
0.030	0.501	0.009	0.687	3.43	1.5	0.072
0.022	0.470	0.007	1.38	2.77	0.72	0.111
0.013	0.360	0.006	1.79	19.6	0.56	0.126
0.008	0.280	0.004	2.32	18.6	0.43	0.146
0.005	0.230	0.003	2.77	13.9	0.36	0.160

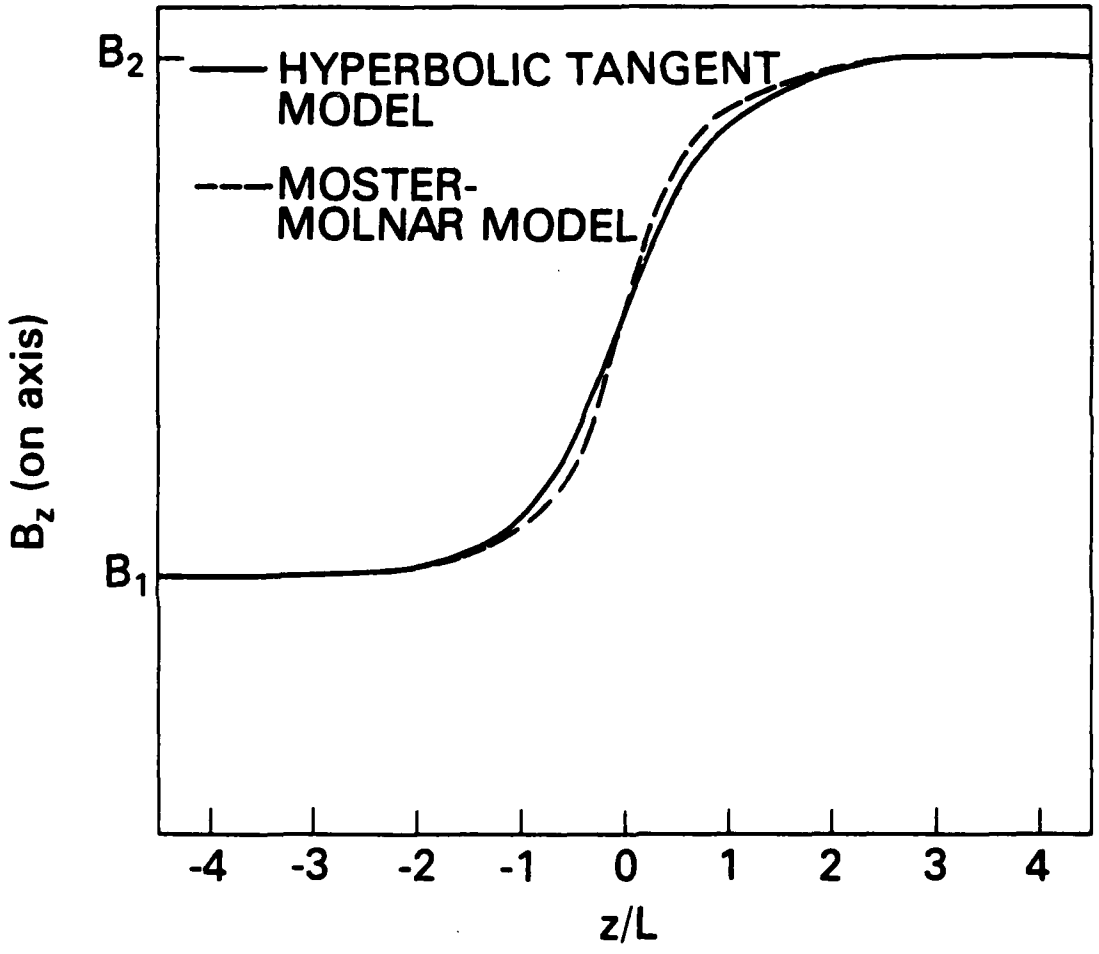

Fig. 1 — Comparison of the two magnetic field models [Eqs. (5) and (9)] used in the electron trajectory calculation.

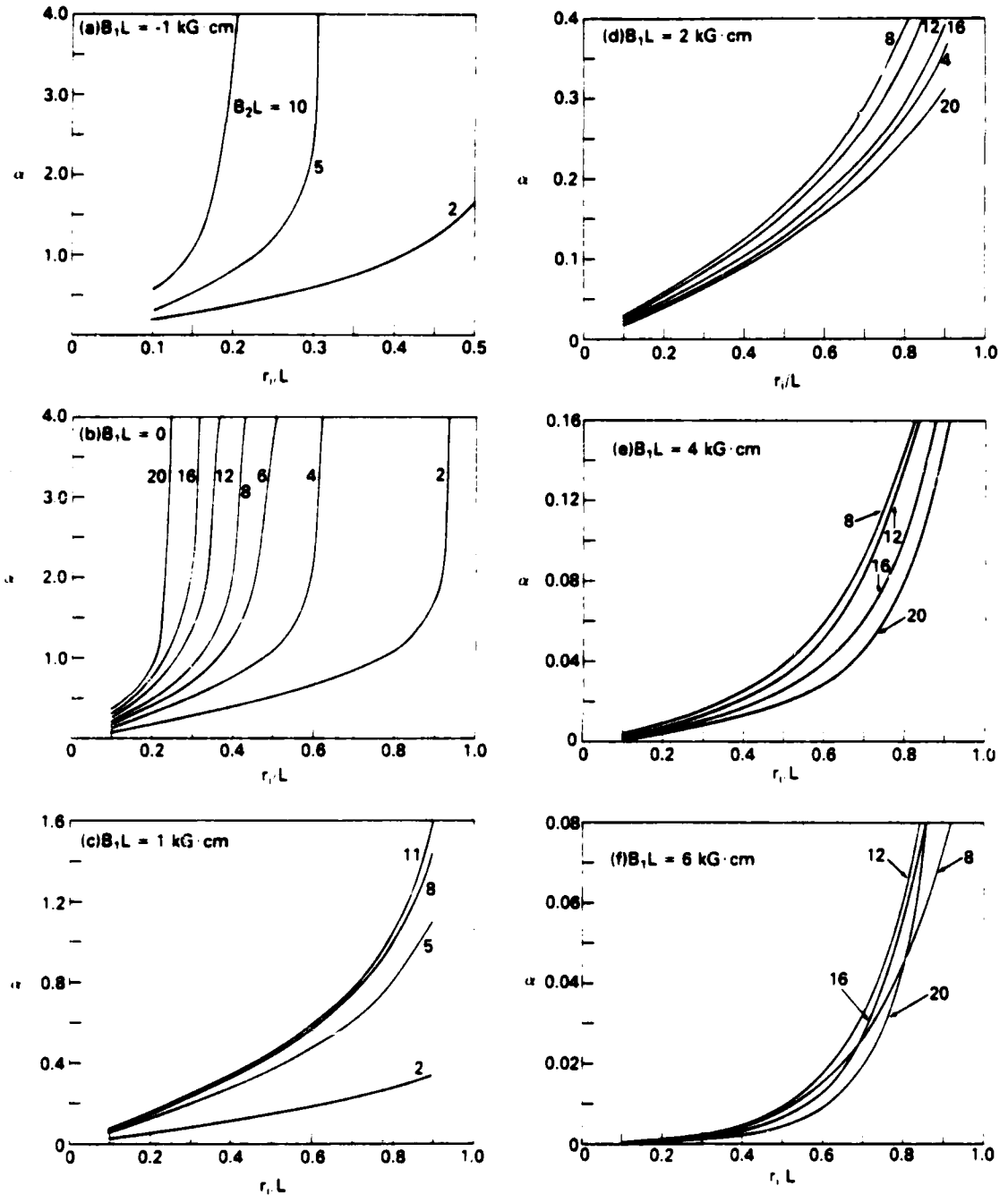

Fig. 2 — α vs the normalized initial electron radial position r_i/L for various $B_1 L$ and $B_2 L$. The numbers attached to each curve are values of $B_2 L$ in unit of kG · cm.

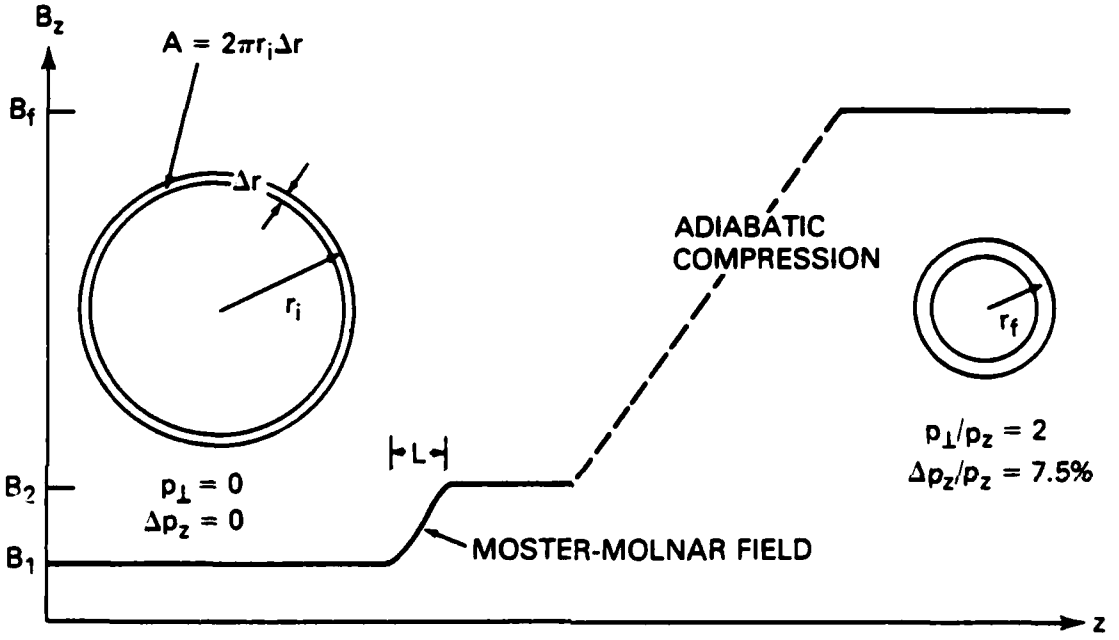

Fig. 3 — A schematic illustration for achieving an electron beam with $\alpha = 2$, $\Delta p_z/p_z = 7.5\%$ in a magnetic field of 50 kG. r_i and Δr are, respectively, the initial average beam radius and thickness. r_f is the final average beam radius. The figure is not drawn to scale. Detailed parameters are provided in Table I.

GYROTRON & ECH DISTRIBUTION LIST

No. of Copies			Addressee
(25) (26)	Naval Research Laboratory Attn: Name/Code 4555 Overlook Avenue, S.W. Washington, D.C. 20375	Code:	4700 - Dr. T. Coffey 4740 - Dr. V.L. Granatstein 4740 - Dr. R.K. Parker 4740 - Dr. K.R. Chu 4740 - Dr. M.E. Read 4740 - Dr. C.W. Roberson 4740 - Dr. S. Gold 4790 - Dr. P.A. Sprangle 4790 - Dr. B. Hui 4790 - Dr. W.M. Manheimer 6850 - Dr. L.R. Whicker 6853 - Dr. A. Ganguly 6805 - Dr. S.Y. Ahn 6805 - N.R. Vanderplaats 6875 - Dr. R. Wagner
	On-Site Contractors:	Code:	4740 - Dr. J.M. Baird (B-K Dynamics) 4740 - Dr. L. Barnett (B-K Dynamics) 4740 - Dr. D. Dialetis (SAI) 4740 - A.J. Dudas (JAYCOR) 4740 - Dr. R.M. Gilgenbach (JAYCOR) 4740 - Dr. K.J. Kim (JAYCOR) 4740 - Dr. Y.Y. Lau (SAI) 4740 - Dr. J.S. Silverstein (HDL) 4790 - Dr. A.J. Drobot SAI) 4790 - Dr. C.M. Hui (JAYCOR) 4790 - Dr. J. Vomvoridis (JAYCOR) 5704S - Dr. S. Smith (LOCUS, Inc.)
(3)	Secretary Department of Energy Attn: Washington, D.C. 20545		Dr. P. Stone (G-234) Dr. M. Murphy (G-234) Dr. J. Willis (G-234)
(1)	Air Force Avionics Laboratory Attn: W. Friz Wright/Patterson AFB, Ohio 45433		
(1)	Bell Laboratories Attn: Dr. W.M. Walsh, Jr. 600 Mountain Avenue Murray Hill, New Jersey 07971		

No. of Copies		Addressee
(1)	Columbia University Department of Electrical Engineering Attn: Dr. S.P. Schlesinger New York, New York 10027	
(1)	Dartmouth College Physics Department Attn: Dr. John Walsh Dartmouth, New Hampshire 03755	
(12)	Defense Technical Information Center Cameron Station 5010 Duke Street Alexandria, Virginia 22314	
(1)	Georgia Institute of Technology Engineering Experimental Station Attn: Dr. James J. Gallagher Atlanta, Georgia 30332	
(3)	Hughes Aircraft Co. Attn: Electron Dynamics Division 3100 Lomita Boulevard Torrance, California 90509	Dr. J.J. Tancredi K. Arnold K. Amboss
(1)	Los Alamos Scientific Laboratory Attn: Dr. Paul Tallerico P.O. Box 1663 Los Alamos, New Mexico 87545	
(1)	Massachusetts Institute of Technology Research Laboratory of Electronics Attn: Dr. G. Bekefi Bldg. 36, Rm. 36-225 Cambridge, Massachusetts 02139	
(3)	Massachusetts Institute of Technology Plasma Fusion Center Attn: 167 Albany St., N.W. 16-200 Cambridge, Massachusetts 02139	Dr. R. Davidson Dr. M. Porkolab Dr. R. Temkin
(1)	Northrop Corporation Defense System Department Electronics Division Attn: G. Doehler 175 W. Oakton St. Des Plaines, Illinois 60018	
(2)	Oak Ridge National Laboratories Attn: P.O. Box Y Oak Ridge, Tennessee 37830	Dr. A. England M. Loring

No. of Copies		Addressee
(1)	Princeton University Plasma Physics Laboratory Attn: Dr. H. Hsuan Princeton, New Jersey 08540	
(2)	Raytheon Company Microwave Power Tube Division Attn: Willow St. Waltham, Massachusetts 02154	R. Edwards R. Handy
(1)	Science Applications, Inc. Attn: Dr. Alvin Trivelpiece 1200 Prospect St. La Jolla, California 92037	
(1)	Stanford University SLAC Attn: Dr. Jean Lebacqz Stanford, California 94305	
(1)	University of Arizona Optical Sciences Center Attn: Dr. W.E. Lamb Tucson, Arizona 85720	
(1)	Varian Associates Bldg. 1 Attn: Dr. H. Jory 611 Hansen Way Palo Alto, California 94303	
(1)	Yale University Mason Laboratory Attn: Dr. J.L. Hirshfield 400 Temple Street New Haven, Connecticut 06520	
(1)	Kings College University of London Attn: Dr. P. Lindsay London, United Kingdom	
(1)	Nagoya University Institute of Plasma Physics Attn: Dr. H. Ikegami Nagoya, Japan 464	
(1)	National Taiwan University Department of Physics Attn: Dr. Yuin-Chi Hsu Taipei, Taiwan, China	

No. of Copies	Addressee
(1)	TFR Group DPH - PFC Attn: Dr. A. Cavallo 92260 Fontenay-auix Roses France
(1)	Thompson C.S.F./DET/TDH Attn: Dr. G. Mourier 2 Rue Latecoere 78140 Velizy Villa conblay France
(1)	UKAEA Culham Laboratory Attn: Dr. A.C. Riviere Abingdon Oxfordshire United Kingdom

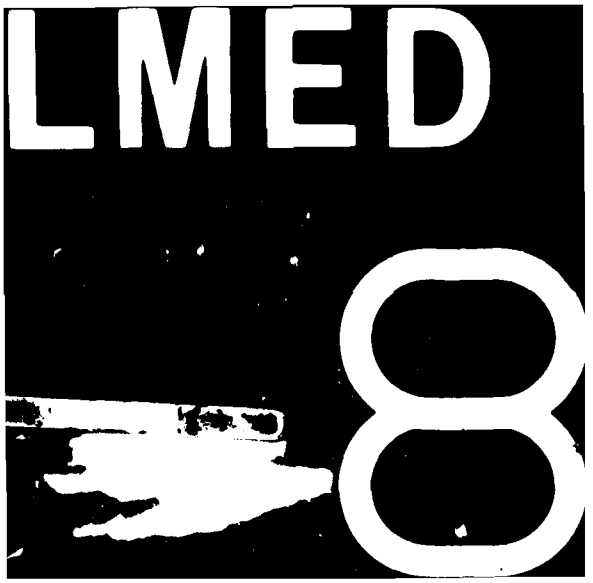
LMED
8